Electrodeposited Mesoporous Pt and Pt@CB Films as Electrocatalysts for the Oxygen Reduction Reactions and Ethanol Electrooxidation in Both Acid and Alkaline Media

Nguyet Doan[1], Tom Sundqvist[1], Panu Hiekkataipale[2], Juuso Korhonen[2], Tanja Kallio[1,*],
Janne Ruokolainen[2], Kyösti Kontturi[1] and Christoffer Johans[1]

[1]Department of Chemistry, School of Chemical Technology, Aalto University, PO Box 16100, 00076 Aalto, Finland
[2]Nanomicroscopy Center, Department of Applied Physics, Aalto University, P.O.Box 15100, 00076 AALTO, Espoo, Finland
[*]E-mail: tanja.kallio@aalto.fi

In this study, mesoporous Pt and Pt@CB were electrodeposited using galvanostatic and potentiostatic methods from liquid crystalline surfactant templates with different amount of Pt (0.25-4.20 mg/m^2). These samples were characterized by SAXS, TEM and SEM in order to understand the growth process and to characterize the end product. Thereafter their potential as electrocatalysts for energy conversion in fuel cells was studied. The oxygen reduction reaction (ORR) is the cathode reaction in fuel cells and because of its importance it has been studed intensively. ORR kinetics is slow and proceed via different meachanism and, consequently, the reaction has been widely investigated in both acidic and alkaline aqueous solutions on different catalysts. Here, ORR on these mesoposous Pt samples was studied using a rotating disk electrode in acidic media and promising results were obtained: The mass activities were better than those of other Pt electrocatalysts reported in the literature: the mass activity for 0.5 mg/m^2 Pt loading was 2.4 A/g$_{Pt}$ at 0.9 V vs. RHE with a rotation rate of 2400 rpm. Ethanol is considered as a promising alternative fuel for portable fuel cells. Hence, the activity of the electrodeposited mesoporous Pt and Pt@CB for ethanol oxidation in alkaline media was also studied and the results showed that mesoporous Pt@CB has a high activity as the onset potentials was sifter 100 mV to more negative potentials than for other Pt based catalyst reported in the literature. These results showed that mesoporous Pt electrocatalyst have also a high potential in direct ethanol fuel cells.

Keywords: mesoporous, Pt, Pt/CB, ORR, CO adsorption, ethanol oxidation, mass activity

1. INTRODUCTION

Oxygen reduction reaction (ORR) is a very important reaction in electrochemical energy conversion devices such as fuel cells. The ORR kinetics is slow and consequently, the reaction

mechanism has been widely investigated in both acidic and alkaline solutions on different electrocatalysts [1, 2, 3]. ORR in aqueous solutions occurs *via* two alternative pathways: the direct four electron transfer pathway from O_2 to H_2O or the two electron transfer from O_2 to hydrogen peroxide (H_2O_2) [1, 4]. Supported Pt nanoparticles in the 3-10 nm size range are the most commonly used catalysts for ORR reactions [5, 6]. It is well-know that the electrochemical activity of Pt catalysts depends on the crystal sites available for reaction, and therefore methods to control the morphology and crystallinity of the Pt has been researched intensively.

Recently, mesoporous Pt and Pt alloys have been found to have promising electrocatalytic activities toward the above mentioned reactions [7, 8]. Hexagonal mesoporous Pt, electrodeposited from a liquid crystalline template, was studied by Attard *et al* [9, 10, 11]. In the preparation, a Pt salt was dissolved into the aqueous phase of a hexagonal lyotropic liquid crystalline template, and subsequently reduced to metal. Elliot *et al.* showed, using the same method, that temperature and deposition potential changes significantly the specific surface area, nanostructure, and macroscopic morphology of the Pt films [12]. Birkin *et al.* studied ORR on hexagonal mesoporous Pt microelectrodes and observed that mesoporous microelectrodes have significantly different oxygen reduction kinetics than polished Pt microelectrodes under otherwise similar conditions [13]. Bauer *et al.* studied ORR on Pt deposited from a liquid crystalline phase template [14]. Rotating disk electrode (RDE) experiments indicated that oxygen reduction performance was improved at a potential more negative than 0.95 V vs. RHE compared to Pt deposited without the template.

Carbon monoxide, a known catalyst poison for Pt, is present in ppm levels in ambient air and consequently CO poisoning of mesoporous Pt cathodes has also been studied widely [15]. Esterle *et al.* used the same method as Birkin *et al.* to produce mesoporous Pt [16]. In their research CO stripping voltammetry on hexagonal mesoporous Pt was significantly different from the corresponding voltammetry on polycrystalline Pt. In the case of mesoporous Pt, there is a clear prewave in the CO stripping voltammogram which accounts for about 15% of the adsorption charge. This was explained by the difference of the concave nature of the surface within the pores.

In direct methanol (DMFC) and direct alcohol fuel cells (DAFC) intermediate CO oxidation is particularly important to avoid poisoning of the anode. Mesoporous Pt has been produced from soft block surfactant templates and used as electrocatalysts in fuel cell applications for methanol oxidation [7, 8, 1, 17]. Franceschini *et al.* studied mesoporous Pt electrocatlysts as methanol tolerant cathodes for DMFCs. In their research, mesoporous Pt was synthesized using a triblock poly(ethene oxide)-b-poly (propylene oxide)-b-poly(ethylene oxide) copolymer (Pluronic F127®) template. They observed a high methanol to CO_2 conversion effiency and high tolerance to CO poisoning [1]. Furthermore, fabrication of Pt nanoparticles supported on mesoporous carbon has been studied as anodic/cathodic electrocalysts in direct methanol fuel cells and hydrogen fuel cells [18, 19, 20, 21].

Because of low toxicity and high energy content compared to methanol, direct electrooxidation of ethanol has attracted more and more attention as an alternative fuel for DAFCs [3, 22]. Ethanol oxidation has been studied on Pt, Pd, PtCo and PtRu nanomaterial catalysts in alkaline electrolytes and ethanol electrooxidation reactions has also been studied on Pt at different temperatures [3, 23 , 24 , 25]. The results showed that in addition to the electrocatalyst material structure, the reaction temperature and concentration of ethanol affects the kinetics of ethanol oxidation. Xu *et al.* studied

methanol and ethanol electrooxidation on Pt and Pd (0.10 mg/cm^2) supported on carbon microspheres in alkaline media [3, 24, 26]. In their studies, it was shown that Pd is a good electrocatalyst for ethanol oxidation in alkaline media.

In this work, we have used a similar method as Attard *et al.* [9, 10] to synthesize mesoporous Pt deposited directly on glassy carbon and on carbon black (Pt@CB) on glassy carbon RDE. ORR, CO oxidation and ethanol oxidation was studied in both acidic and alkaline media. ORR activity of mesoporous Pt structures was observed to be better than that of nonporous Pt and especially the performance in the electrooxidation of ethanol was superior on the mesoporous material. To our knowledge, electrooxidation of ethanol on this type of porous Pt has not been reported previously.

2. EXPERIMENTAL

2.1. Chemicals

The surfactant Brij®C10 (Aldrich), hexachloroplatinic acid hydrate (HCPA, 99.9%, Aldrich), ethanol (Etax A, 96.1 vol-%, Altia), NaOH (Merk), HClO$_4$ (Merck), Vulcan XC72R (Cabot GR-3875), 5 wt. % Nafion® dispersion in low molecular weight alcohols (Aldrich) were used. The gases (N$_2$, synthetic air, CO) were all produced by AGA with at least 99.99% purity. Ion-exchanged Millipore Milli-Q water was used for solutions and cleaning electrodes.

2.2. Electrodeposition of Pt structures

The substrate was a glassy carbon (GC) rotating disk electrode (RDE, d=5mm, Pine Instruments), which was polished in three stages. First the substrates were polished with grinding paper (P600 roughness, Carbimet® Paper Disc) and alumina slurries (Micropolish®Alumina) of 1 and 0.05 μm particle size, and finally, the electrodes were sonicated in high purity water and after that in ethanol for approximately one hour.

The plating mixture contained 29 wt% HCPA, 45 wt% Brij®C10 and 26 wt% water. The mixture was stirred with a plastic spatula and heated in a sealed vial to 40 ˚C for 30 min, this process was repeated twice. The colour of the mixture was bright orange and it was used within one week from the preparation. The platinum plating mixture was deposited onto the GC electrodes using a PTFE cap with a hole matching the electrode diameter and sealed with parafilm. The electrode system was put into a sealed vial and placed into an oven at 40 ˚C for 2 hours. The mixture was slowly cooled down with an approximate rate of 4 ˚C/h to 20 ˚C, to make sure that liquid crystal phase were well organized, see SAXS analysis. The same procedure was also used for the TEM analysis, however, using carbon coated TEM grids (Electron Microscopy, 400 mesh copper formvar/carbon) as the substrate [14]. The carbon coated side of the grid was used for the electrodeopsition.

Deposition of Pt was done also using carbon black (CB, Vulcan XC72R) as a support and Nafion® (Aldrich) ionomer as a binder. The CB support was pretreated in N$_2$ flow at 300 ˚C for 2 hours and then deposited on the GC substrate (diameter 5 mm). Briefly, 5 mg of the purified CB powder was dispersed in 200 μl of 96.1 vol-% ethanol and 20 μl of 5 wt. % Nafion ionomer dispersion

was added. The solution was stirred with a magnetic stirrer for an hour and sonicated for another hour resulting in a black ink solution. The solution was cast on the GC surface and dried overnight under ambient conditions. Electrodeposition was performed with a deposition current of -500 µA varying the used charges, and alternatively, in potentiostatic mode at -175 mV vs. SCE with a Pt wire/gauze as a counter electrode and a Dri-Ref (World Precision Instruments, Inc.) as a reference electrode. The potential of the Dri-Ref electrode is 20 mV vs. SCE in 0.05 M H_2SO_4. After electrodeposition, the surfactant template and reactants were removed by immersing the working electrode in a mixture of water and ethanol (1:1) for approximately 3 h and after that the solution was exchanged and the electrode was kept in the solution of water and ethanol for one more hour.

2.3. Characterization of mesoporous Pt and Pt@CB

Before electrodeposition, the phase of the mixture was characterized using the small angle X-ray scattering (SAXS) and A JEOL FEM-3200FSC cryo transmission electron microscopy (cryo-TEM). The SAXS setup consists of a Bruker Microstar microfocus rotating anode X-ray source with Montel collimating Optics (parallel beam, Cu Kα radiation λ = 1.54 Å), where the beam was further collimated using three sets of JJ X-ray 4-blade slits. The diameter of the beam was 0.8 mm at the sample position. A sample-to-detector distance of 59 cm was used. The scattering intensities were measured using a 2D area detector (Bruker HiStar). The samples were sealed in a metal holder between two 7 □m Kapton films to yield a sample with a thickness of approximately 0.1 mm. The measurements were done at room temperature of 23 ˚C in helium atmosphere. One-dimensional SAXS data were obtained by azimuthally averaging the 2D scattering data. The magnitude of the scattering vector is given by $q = (4\pi/\lambda) \sin \theta$, where 2θ is the scattering angle. Standard corrections for sample absorption and background scattering were performed. For cryo-TEM characterization, the sample gel was frozen in liquid nitrogen and subsequently sectioned at -100 °C to thin 70 nm slices using a Leica UC7/FC7 cryo-ultramicrotome with a 35° Diatome cryo diamond knife. Sections were gathered onto a lacey carbon 200 mesh copper grid (SPI Supplies). The sample grid was transferred into the cryo-TEM while preserving the sample at liquid nitrogen temperature at all times. The microscope was operated at liquid nitrogen temperature and imaging was performed with 300 keV electron energy. Zero-loss energy-filtered micrographs at slight under-focus were gathered using low-dose conditions, as the sample was prone to beam damage. The mesoporous Pt samples were examined using transmission electron microscopy (TEM) and scanning electron microscopy (SEM JSM-7500F) coupled with energy-dispersive X-ray spectroscopy (EDS). The TEM samples were prepared by electrodepositing Pt directly onto carbon grids (Electron Microscopy Sciences, 400 meshes). The measurements were done with a Tecnai 12 instrument operating at 120 kV accelerating voltge.

2.4. Electrochemical characterization of mesoporous Pt and Pt@CB

All experiments were performed with an Eco Chemien Autolab PGSTAT12 potentiostat. The counter electrode was a Pt wire and the reference electrode was a SCE. The mesoporous Pt surface was

cleaned electrochemically by cycling several times between -0.20-0.45 V vs. SCE in 0.1 M HClO$_4$ at 25 ˚C at a sweep rate of 20 mV/s before the electrochemical measurements. The following electrochemical experiments were done on mesoporous Pt and Pt@CB: cyclic voltammetry (CV), CO adsorption, oxygen reduction reaction (ORR) with the different rotation rates in both acidic and alkaline media and oxidation of ethanol in alkaline media. The last meantioned were measured vs. a Hg/HgO reference electrode. For studying CO adsorption on mesoporous Pt and Pt@CB, the cell was purged with CO for 30 minutes holding the electrode potential at 0.25 V vs. SCE at a rotation rate of 300 rpm to complete CO adsorption. Then the cell was purged with nitrogen for 30 minutes to remove CO from the solution. The samples were cycled, between -0.15 V and +0.80V vs. SCE, beginning from -0.15 V to positive direction, at a rate of 10 mV/s. The charge passed was determined by integrating the area between a CO oxidation peak and the background current and using a surface area to a charge ratio of 420 µC/cm^2 [27]. The potential in the electrodepositions and all the other electrochemical measurements used in this study were converted to the reversible hydrogen electrode (RHE) scale.

3. RESULTS AND DISCUSSIONS

3.1. Electrodeposition

Deposition of mesoporous Pt was first studied using a cyclic voltammetry at a scan rate of 0.01 V/s to determine the relevant deposition potentials. The open-circuit potential was always approximately 0.7 V vs. RHE; onset potential for the reduction of Pt was around -0.15 V vs. RHE, see Figure 1.
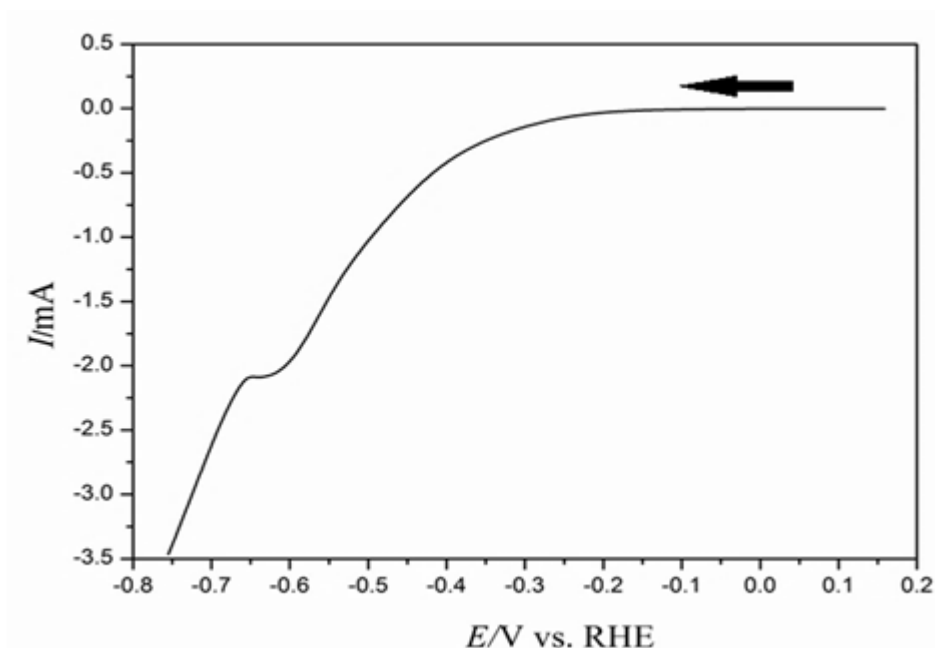
Figure 1. Deposition of mesoporous Pt using linear sweep voltammetry at a scan rate of 0.01 V/s.

Depositions of mesoporous Pt were done on a glassy carbon (GC) and carbon black deposited on glassy carbon electrodes (CB/GC) with a constant current of -2.5 mA/cm^2 (galvanostatic) and a constant potential of -175 mV (potentiostatic) with deposition charges varying from 0.50 to 8.35 C/cm^2. Of these two deposition methods galvanostatic resulted in more stable electrodes on GC and therefore, was used for further on GC. However, the electrodeposition of mesoporous Pt on carbon black, Pt@CB, was done potentiostatically because the adhesion was better than that obtained with the galvanostatic method. Investigation of the origing of this behaviour is, however, out of the scope of this study. The deposition charges and theoretical masses with the used deposition method of the materials selected for further studies are shown in Table 1.

Table 1. Deposition charge, theoretical mass for electrodeposited Pt and Pt mass per geometrical area of the electrode using a constant current of -2.5 mA/cm^2 (galvanostatic) and constant potential of -175 mV (potentiostatic).

| Sample	Q/A C/cm^2	mPt mg	mPt mg/m^2	Deposition method
A$_{GC}$	0.5	0.05	0.25	Galvanostatic
B$_{GC}$	1	0.10	0.50	Galvanostatic
C$_{GC}$	2	0.20	1.00	Galvanostatic
D$_{GC/CB}$	2	0.20	1.00	Potentiostatic

3.2. Cryo-TEM, SAXS, TEM and SEM characterization

Figure 2 presents the measured and calculated SAXS patterns of the mesoporous Pt plating mixture before the electrodeposition. The experimental scattering pattern (dotted black line) coincides well with two theoretical ones of lamellar and hexagonal crystal phases (solid blue and red lines). Based on these experimental and calculated data, it appears that mesoporous crystal liquid consists of two different structures, lamellar structures with a lattice vector of 6.4-6.5 nm and hexagonal structures with a lattice vector of 6.7-6.8 nm. The size of the lattice parameters measured by SAXS is in good agreement with those obtained from cryo-TEM (see Figure 3) and TEM (Figure 4) analysis. The cryo-TEM results (Figure 3a) show that there are lamellar structures with a lattice vector of 6-7 nm. However, also other structures can be observed as shown in Figure 3b (enlarged figures are avaible in supporting information, Figure S1 and S2). These structures do not appear to be hexagonal, as indicated by the SAXS analysis, but rather irregularly organized structures of the surfactant aggregates. We point out that many structures can give similar response in the SAXS, and hence the sensitivity in this case may not be sufficient for determining the prevailing structures at the resolution available with our instrument.
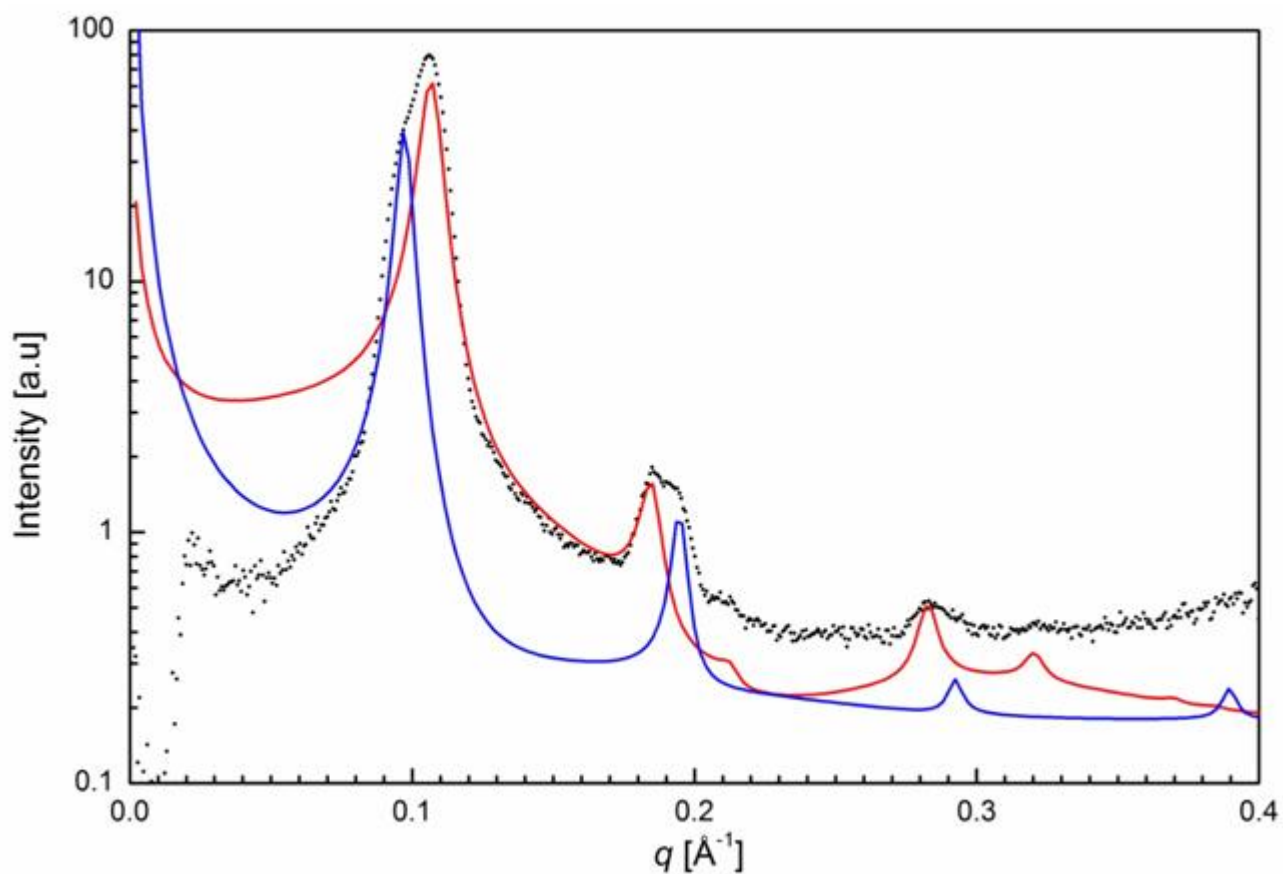
Figure 2. SAXS pattern of Pt mesoporous mixture before electrodeposition at 23˚C in helium atmosphere. Dottedblack line: measured data, solid blue line: calculated lamelle fitting (lattice crystal is 6.45 nm), solid red line: calculated hexagonal fitting (lattice crystal is 6.79 nm).
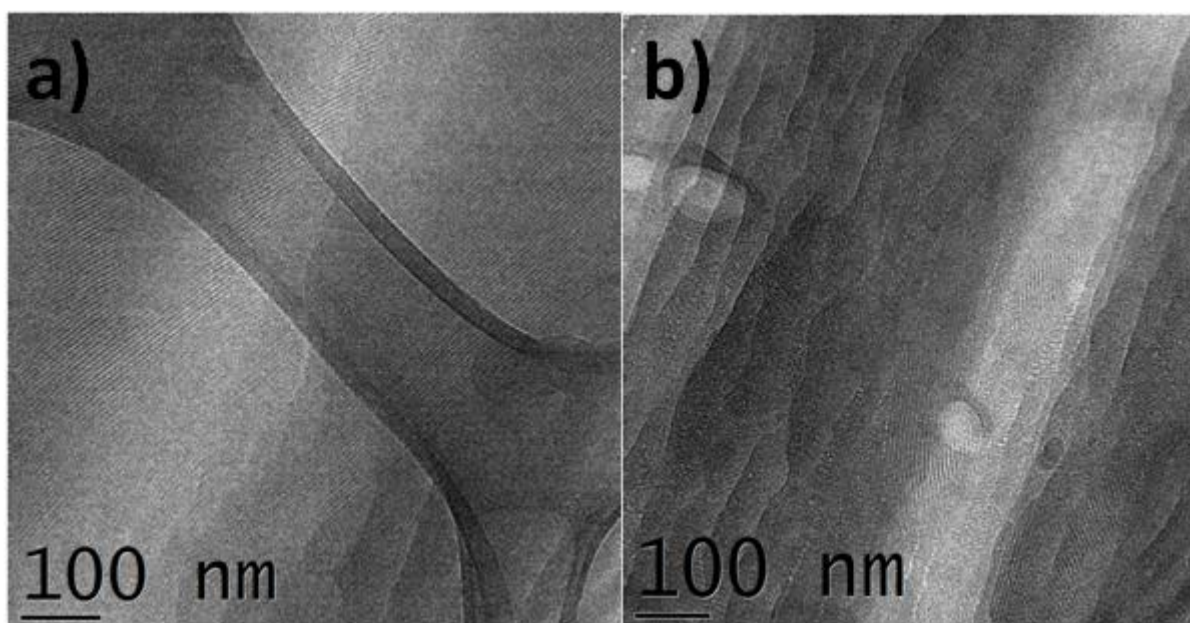
Figure 3. Cryo-TEM images of the mesoporous liquid crystal.

Mesoporous Pt electrodeposited from the surfactant templates are shown in Figure 4. In Figure 4a islands with a nearly circular outline can be seen with outer diameters in the 50-400 nm range. Figure 4b shows an island in the initial growth stages. The porous structure of the deposits can be clearly observed, with pores in the 3-5 nm range. These pores are separated by 5-8 nm irregular shapes of Pt. Contrary to the work of Attard *et al.* [9, 10] the pores are not hexagonally oriented, but rather irregular and reminiscent of the irregular surfactant structures observed with TEM, see above. We have chosen this morphology due to the complex topology that may provide interesting defect characteristics and consequently catalytic activity.

On the bases of TEM images taken of mesoporous Pt at different growth stages, it seems that islands consisting of a thin porous Pt layer initially forms on the electrode surface, see Figure 4a. In the next step three dimensional growth takes place, usually starting from the edge of the deposit and growing back over the film, see e.g. the lower right quadrant in Figure 4a. The nucleation of new islands seems to be a progressive process since longer deposition time leads to a higher number density of islands, with persistent observation of thin deposits. The reader should be aware that the surface properties of the glassy carbon and carbon black substrates used in the catalysis experiments may not be perfectly represented by the carbon coated TEM grid. Therefore, differencies in morphology may occur. We did not observe lamellar deposits, which suggest that this morphology is unfavourable for electrodeposition.
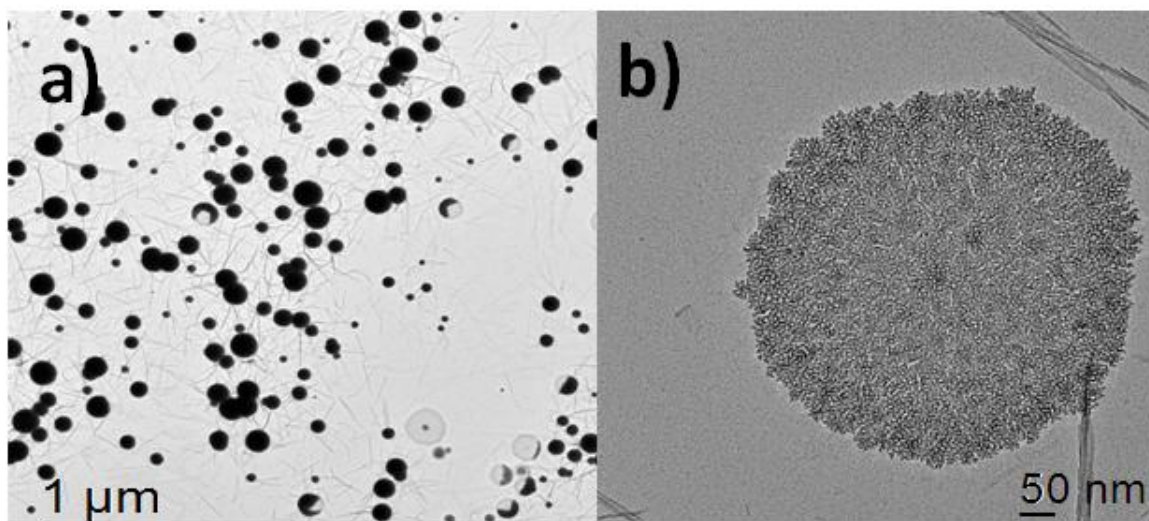
Figure 4. TEM images of the electrodeposited Pt directly onto formvar/carbon grids with -0.5 mA constant current.

The SEM images in Figure 5 show that structures on the glassy carbon RDE electrodes form aggregated spherical particles with diameters in range of 100-500 nm. The deposits were also characterized by EDS for both the mesoporous Pt on GC and Pt@CB showing that the sample contains both Pt and C as expected, see Supporting information and EDS elemental spectrum shown in Figure S3. The accurate ratio of Pt and C cannot be determined because the sample was electrodeposited on

glassy carbon electrode affecting the EDS analysis. The elemental distribution of these samples are shown in Figure 6. Bauer *et al.* have also studied mesoporous Pt synthetized using Brij®56 which is the same surfactant as in our work. They observed that when a small amount of heptane (3 wt.-%) was added to the mixture, the pores in the particles appear to be hexagonally arranged whereas the pores obtained without heptane were not arranged in a structured manner in agreement with our results [14]. Furthermore, Elliot *et al.* has shown earlier that also the used temperature and deposition potential affect the structure of mesoporous Pt. The most ordered nanostructures were observed when the deposition potential was more negative than -0.2 V vs. SCE at 25 ˚C. [12]
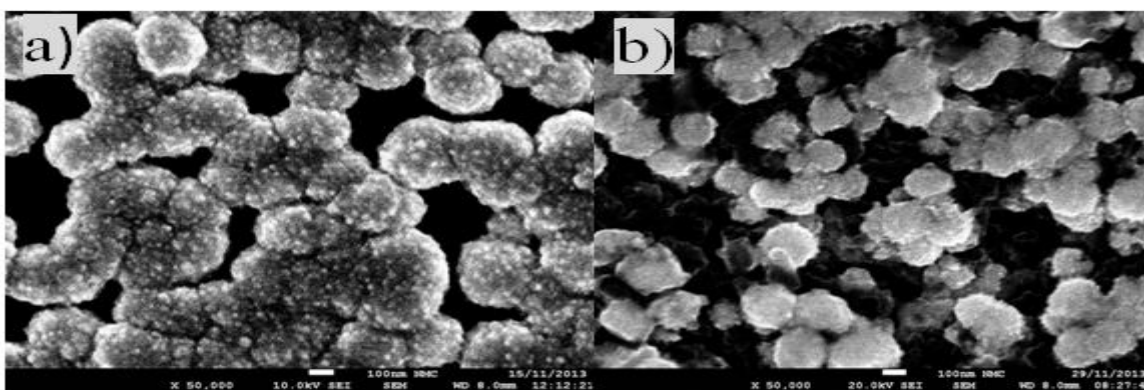

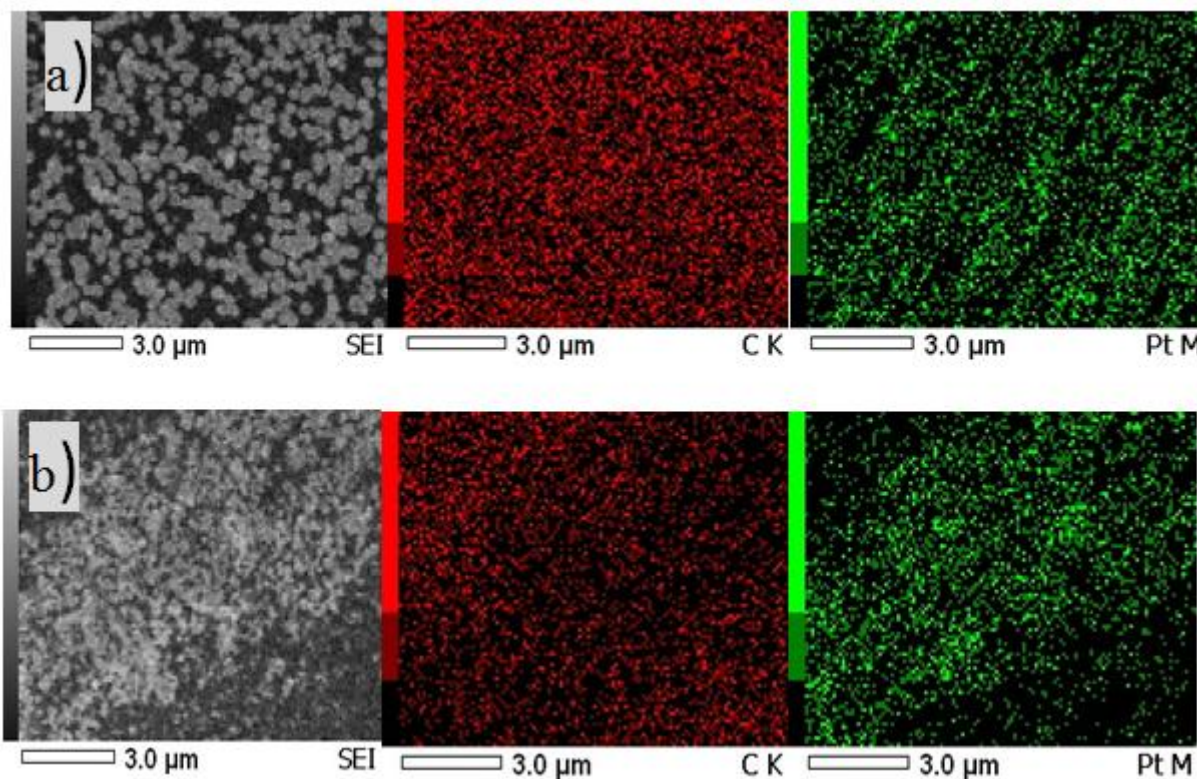**Figure 5.** SEM images of mesoporous a) Pt (1 C/cm^2) and b) Pt/CB (2 C/cm^2).

Figure 6. SEM images of elemental (Pt and C) distribution of mesoporous a) Pt and b) Pt/CB.

*3.3. Voltammetric and CO desorption characterization of mesoporous Pt and Pt@CB in both acid and alkaline media*

A cyclic voltammogram recorded at 20 mV/s for mesoporous Pt, (sample C_{GC}) in 0.1 M $HClO_4$ is shown in Figure 7. Hydrogen adsorption and desorption on nanoparticles and mesoporous Pt electrodes in H_2SO_4 have been thoroughly studied [16, 14] but there are only few studies in $HClO_4$ [28, 29]. The hydrogen adsorption/desorption peaks can be observed at 0.05, 0.25 and 0.28 V vs. RHE, as typical for polyoriented Pt. The electrochemical active surface area (EASA) was determined using the charge of the hydrogen adsorption/desorption region, corrected for double layer charging by standard procedure, and using 200 μC cm^{-2} as a charge density of a monolayer of hydrogen [27, 29] on polyoriented platinum surface. For the sample C_{GC} the electrochemically active interfacial area is 7.4 m^2/g and the rugosity 75.0. Clearly higher EASAs of 56-66 m^2/g have been reported for Pt/Vulcan XC72 nanoparticle based catalysts [30]. The reason for this difference is the smaller particle size in the 2-4 nm range of that catalyst in comparison to the mesoporous structures with a diameter of 50-400 nm (see Figure 4a and 4b).
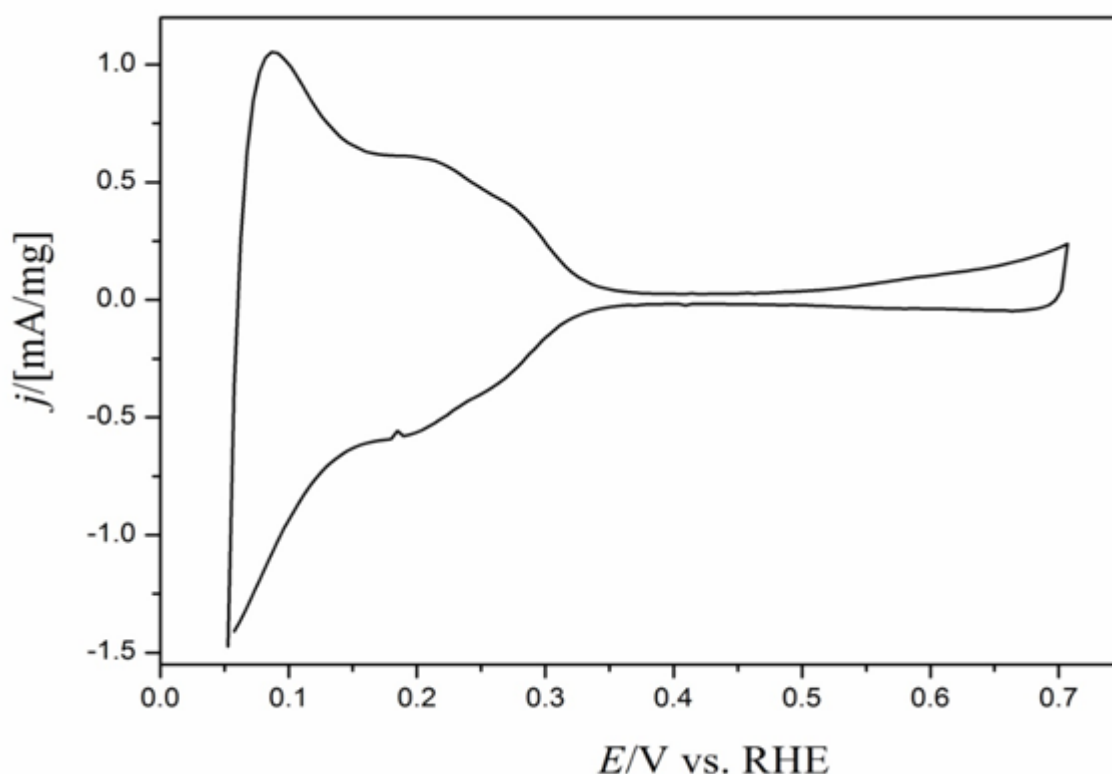
Figure 7. Cyclic voltammograms of electrodeposited mesoporous Pt, sample C_{GC}, in 0.1 M $HClO_4$.

The sweep rate was 20 mV/s. The current was normalized with the total metal loading on the electrode. CVs recorded for the mesoporous Pt samples B_{GC} and $D_{GC/CB}$ in 0.1 M NaOH are shown in Figure 8. The CV exhibits hydrogen underpotential deposition peaks at 0.27 and 0.35 V and surface hydroxide peaks at 0.52 V and 0.76 V vs. RHE typical for Pt. The CVs for both samples resemble each

other and major differences can be observed at high potentials (*ca.* 0.7-1.2 V) where surface oxides are formed. The higher currents detected for the $D_{GC/GB}$ in the so called double leyer region can be attributed to the Vulcan XC72 support with a high specific surface area in comparison to the mesoporous Pt. The difference in the magnitude of the currents at the high potentials reflect the difference in the deposited amount and morphology of the Pt and the support material as currents normalized against mass of Pt in the hydrogen adsorption/desorption region are very similar indicating similar mass specific surface area and similar ratio of the different Pt planes. Indeed, the surface area calculated, from the adsorption of hydrogen, for the B_{GC} sample are 8.2 m^2/g and the roughness factors of 42 and for $D_{GC/CB}$ the corresponding values are 7.6 m^2/g and 77, using 145 µC cm^{-2} as a charge density for an adsorbed monolayer of hydrogen typically used in alkaline solutions [29]. According to these results EASAs of samples C_{GC} and $D_{GC/CB}$ are very close to each other in both acid (7.4 m^2/g) and alkaline media (7.6 m^2/g) as expected. Futhermore, it is observed that the porosity in sample $D_{GC/CB}$ is higher than in the samples deposited on bare glassy carbon suggesting that the morphology of the support and/or the depositon method affects the morphology of the mesoporous Pt.
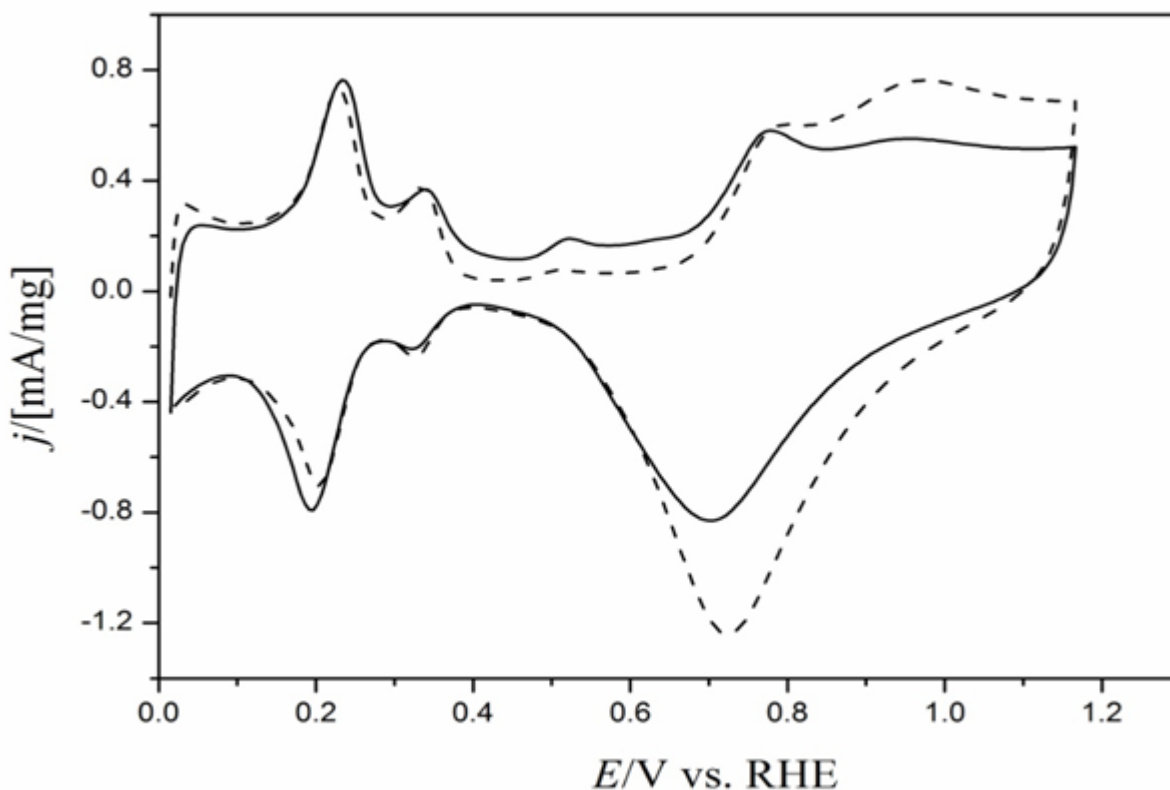

Figure 8. Cyclic voltammogram of samples B_{GC} (dash) and $D_{GC/CB}$, (solid) in 0.1 M NaOH. The sweep rate was 20 mV/s. The current was normalized with respect to the total metal loading on the electrode.
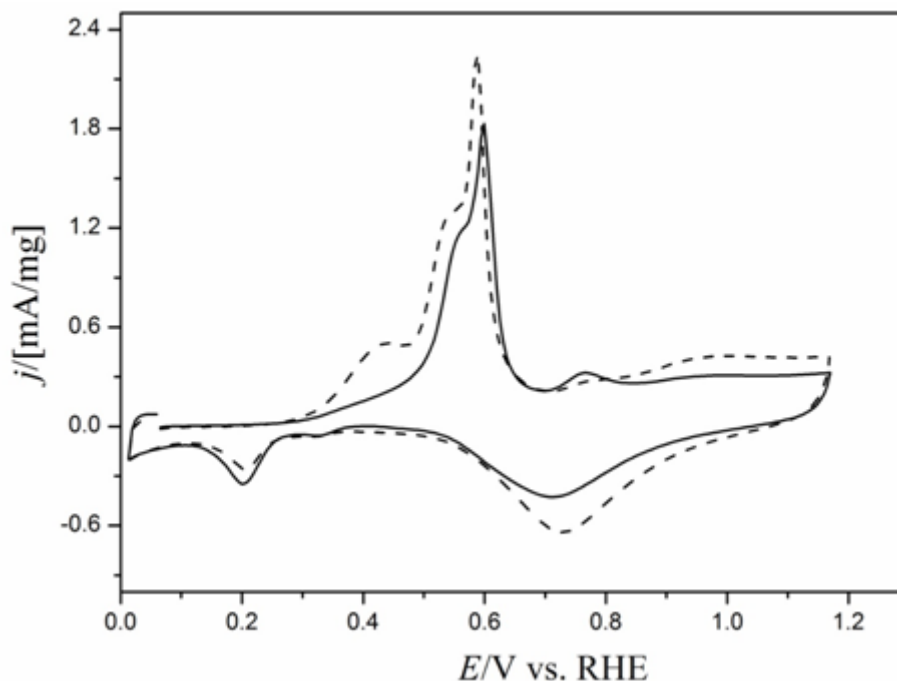
Cyclic voltammograms of samples B_{GC} and $D_{GC/CB}$ in this work resemble those of preferentially oriented spherical Pt nanoparticles in the study by Feliu *et al.*[29]. In their work different shapes of Pt nanoparticles with different preferential orientations were investigated in both acid and

alkaline electrolytes. Their spherical particles were observed to consist of 6% of Pt(111) and 14% of Pt(100) sites suggesting that our mesoporous Pt also have these sites. However, the morphologies of these particles differ notably as the particles are porous in our case (see Figure 4), forming big flower-like structures of spherical particles with diameters in range of 50-400 nm and the pores in the 3-5 nm range as discussed above, contrary to spherical particles in the work by Feliu *et al.*

The mesoporous Pt samples were further characterized using CO adsorption/oxidation method. CO stripping voltammograms recorded in 0.1 M $HClO_4$ for the samples A_{GC} and C_{GC} are shown in Figure 9. No features corresponding to hydrogen desorption from the CO covered surface were observed indicating that CO is able to block H_2 adsorption sites as commonly found for polycrystalline Pt. The CO stripping peaks for the mesoporous Pt samples are approximately at 0.79 V. The onset potentials and peak current densities for the samples A_{GC} and C_{GC} are 2.84 mA/mg$_{Pt}$ and 4.26 mA/mg$_{Pt}$ at the potentials of 0.72 V and 0.68 V, respectively. The CO stripping peaks of the samples A_{GC} and C_{GC} resemble those observed by Esterle and co-workers [16]. They used $C_{12}EO_8$ or $C_{16}EO_8$ as surfactants and sulphuric acid as an electrolyte, instead of Brij®C10 and perchloric acid as reported here. However, they observed that the main CO stripping peak on mesoporous Pt consisted of a peak at 0.7 V with a small shoulder at 0.74 V vs. RHE, instead of one main CO stripping peak, as in our work.
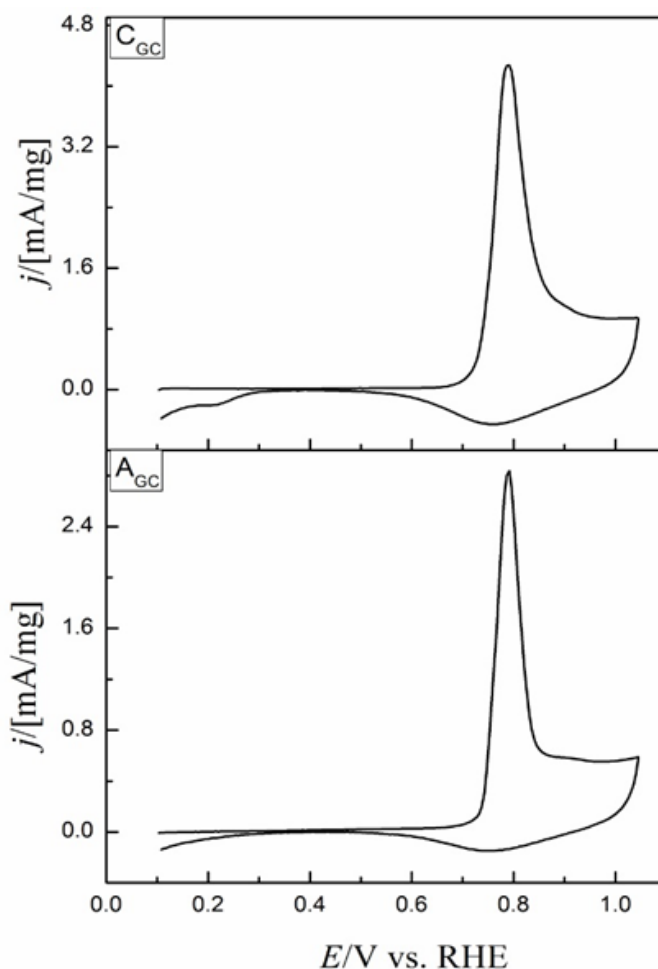
Figure 9. Cyclic voltammograms of CO desorption on mesoporous Pt in 0.1 M $HClO_4$ solution with various loaded Pt: sample A_{GC} 0.050 mg and sample C_{GC} 0.20 mg. The current was normalized with the total metal loading on the electrode.

Figure 10. Cyclic voltammograms of CO desorption on sample B_{GC} (dash curve) with 1 C/cm^2 and sample $D_{GC/CB}$ (solid curve) with 2.0 C/cm^2 charges in 0.1 M NaOH. The current was normalized to the geometric area of the electrode.

CO oxidation on the samples B_{GC} and $D_{GC/CB}$ was also studied also in alkaline media. The CO stripping voltammograms for these samples recorded in 0.1 M NaOH solution are shown in Figure 10. The CO desorption peaks in alkaline media differ from those in acidic environment. The onset potential and the peak potential are observed at lower potentials as expected, 0.24 V and 0.59 V for the sample B_{GC} and 0.26 V and 0.61 V for the sample $D_{GC/CB}$. Furthermore, three voltammetric peaks were observed for the CO oxidation process on the sample B_{GC}, at 0.43 (prepeak), 0.54 and 0.59 V and two peaks for sample $D_{GC/CB}$ at 0.57 and 0.61 V. These results resemble CO stripping voltammetry studies for Pt nanoparticles on carbon black in alkaline media by Kokoh *et al.* [31]. The multiple peaks for CO stripping at different potential regions can be explained by CO on different adsorption sites as this process is known to be very surface site sensitive [32]. The mesoporous Pt sample ($D_{GC/CB}$ 77 cm^2_{active} $_{Pt@CB}cm^{-2}_{geom}$ and B_{GC} 42 $cm^2_{active\ Pt}cm^{-2}_{geom.}$) seems to have better CO activity than the conventional Pt@CB sample which can be explained by the higher porosity.

CO adsorption/desorption is commonly used as an alternative method to determine the electrochemical active surface area of Pt [33, 34]. The charge passed during CO desorption, Q_{CO}, is obtained by integrating the area between the CO oxidation peak and the background using data from Figures 9 and 10. The surface area is estimated using the formula:

$$S = \frac{Q_{CO}}{\theta_{COads} \cdot Q_{COmono}}$$ (1)

where the θ_{COads} is the surface coverage of the CO on the catalyst. Different θ_{COads} values has been reported from 0.60 to 0.80 in the potential range of 0.50-1.05 V vs. RHE depending on the orientation of CO on the surface [27]. Q_{COmono} is the charge needed to deposit monolayer of CO molecules on the catalyst surface and here we have used 420 μC cm^{-2} [27] . In this study we chose to use 0.75 for θ_{COads} commonly used for polycrystalline Pt [35]. Deposition charge, corresponding electrochemical surface active area and mass specific surface area in 0.1 M HClO$_4$ and 0.1 M NaOH for both hydrogen and CO desorption are shown in Table 2.

Table 2. Deposition charge, corresponding electrochemical surface active area and mass specific surface area in 0.1 M HClO$_4$ and 0.1 M NaOH for both hydrogen and CO desorption.

| Catalyst	Charge C/cm^2	Electrolyte 0.1M	Surface active area cm^2	Mass specific surface area m^2/g
Hydrogen desorption				
Sample B$_{GC}$	1	NaOH	8	8.2
Sample C$_{GC}$	2	HClO$_4$	14.7	7.4
HYPERLINK "mailto:Pt@CB" Sample D$_{GC/CB}$ *	2	NaOH	15	7.6
CO desorption				
Sample A$_{GC}$	0.5	HClO$_4$	3.6	7.2
Sample B$_{GC}$	1	NaOH	7.4	7.5
Sample C$_{GC}$	2	HClO$_4$	21.2	10.8
HYPERLINK "mailto:Pt@CB" Sample D$_{GC/CB}$ *	2	NaOH	6.7	10.6

*Potentiostatic electrodeposited sample.

3.4. Oxygen reduction reactions analysis by RDE in acid media

The voltammograms of samples A$_{GC}$, B$_{GC}$, and C$_{GC}$, for oxygen reduction in an O$_2$-saturated 0.1 M HClO$_4$ aqueous solution at room temperature are shown in Figure 11 (sweep rate of 5 mV/s and rotation rate 2400 rpm). Oxygen reduction experiments were also performed with various rotation rates in 0.1 M HClO$_4$ aqueous solution at 25 ˚C. The RDE voltammograms for galvanostatic electrodeposited mesoporous Pt with 2.0 C/cm^2 charges, sample C$_{GC}$ with different rotation rates can be seen in Figure S4 (see supporting information).

A set of the applied voltage (E_{appl}) values between 0.40 V and 0.80 V were chosen to plot the Koutecky-Levich (KL) [36] curves. KL plots at various potentials for sample C$_{GC}$ can be seen in Figure S5 (see supporting information). The number of the electrons (n) transferred were calculated using equation (1) with the data from Figure S4 (see Supporting information). The number of electrons

for all the samples were close to 4 as expected, indicating a primary mechanism leading H_2O, as has been well established for platinum in numerous studies.

Bauer *et al.* synthesized mesoporous Pt on Au electrode using the same method and the same surfactant as in our work [14]. In their studies it was shown that a mass activity (A/g_{Pt}) value for non-templated Pt on gold was 0.5 and for templated Pt on gold was 1.5, which is slightly lower than our samples B_{GC} (2.4 A/g_{Pt}). Furthermore, the onset potential of samples B_{GC} is shifted about 60 mV to more positive compared to their electrodes indicating our electrode higher catalytic activity toward ORR. Kucernak *et al.* studied ORR on mesoporous Pt (H_I-Pt) using a microelectrode and the mass activity was also lower (1.1 A/g_{Pt}) than in our work at 0.9 V vs. RHE [37]. Higuchi *et al.* [36] obtained higher mass activity values (17 A/g_{Pt}) which can be expected because the catalysts were Pt nanoparticles on carbon and carbon black supports resulting in higher active surface area. A comparison of ORR activity with published data, obtained under similar conditions, is shown in Table 3.
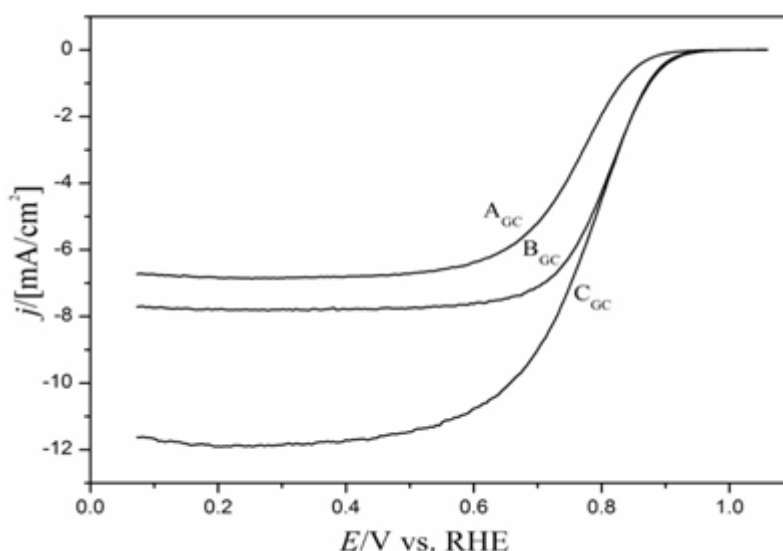
Figure 11. Current-potential curves for oxygen reduction in in an O_2-saturated 0.1 M $HClO_4$ aqueous solution at room temperature. The sweep rate was 5 mV/s and rotation rate 2400 rpm. Curves are: sample A_{GC}, 0.5 C/cm^2, sample B_{GC}, 1.0 C/cm^2, and sample C_{GC}, 2.0 C/cm^2. The current was normalized to the geometric area of the electrode.

Table 3. Comparison of ORR activity at 0.9 V vs. RHE.

RDE type	Mass activity A/g_{Pt}	Onset pontential E_s	Rotation rate rpm	Scan rate mV/s	Electrolyte	T ˚C	Reference
Sample A_{GC}	1.1	0.87	2400	5	0.1 M $HClO_4$	25	This work
Sample B_{GC}	2.4	0.91	2400	5	0.1 M $HClO_4$	25	This work

Sample C$_{GC}$	1	0.91	2400	5	0.1 M HClO$_4$	25	This work
Nontemplated Pt/Au	0.5	0.88	2500	2	0.5 M H$_2$SO$_4$	25	[20]
Templated Pt/Au	1.5	0.92	2500	2	0.5 M H$_2$SO$_4$	25	[20]
mesoPt (H$_I$-Pt)	1.1	0.98	2500	1	0.5 M H$_2$SO$_4$	20	[32]
CB supported Pt	17	0.97	1500	10	0.05 M H$_2$SO$_4$	30	[33]

### 3.5. Oxidation of ethanol on Pt and Pt@CB in alkaline media

Cyclic voltammograms of ethanol oxidation in 1.0 M EtOH+0.1M NaOH on mesoporous Pt@CB and Pt electrodes are shown in Figure 12. The onset potential for ethanol oxidation is 0.24 V on Pt@CB (2.0 C/cm^2, ~1.0 mg/cm^2) and on Pt (1.0 C/cm^2, ~0.50 mg/cm^2) 0.25 V vs. RHE. To our knowledge, electrooxidation of ethanol on this type of mesoporous Pt in alkaline media has not been reported previously, howerever Xu *et al.* studied methanol and ethanol electrooxidation on Pt and Pd (0.10 mg/cm^2) on carbon microspheres in alkaline media. In their studies, it was shown that Pd is a good electrocatalyst for ethanol oxidation in alkaline media. [24] Later on the same group studied electrooxidation of various alcohols on Pt and Pd electrodes in alkaline medium [38]. They observed a good activity for methanol electrooxidation on the Pt electrode but bad on the Pd electrode.
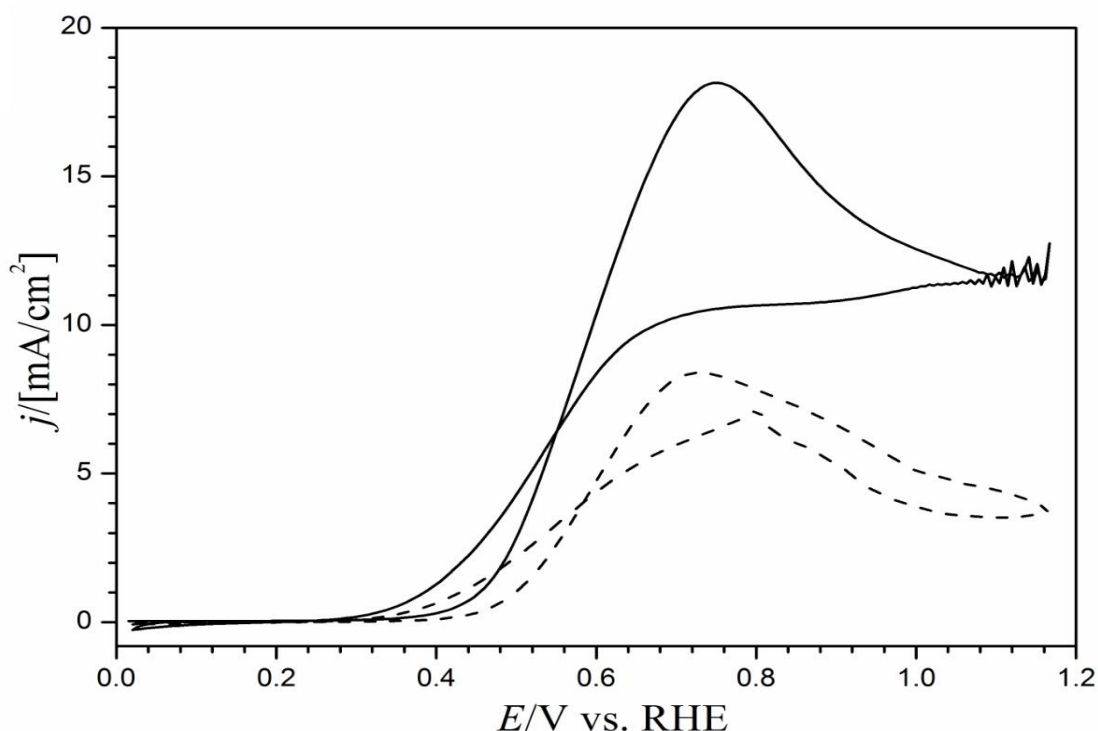
Figure 12. Cyclic voltammograms of electrodeposited Pt@CB (solid) with 2.0 C/cm^2 charge and Pt (dash) with 1.0 C/cm^2 charge in 1.0 M EtOH+0.1M NaOH. Sweep rate was 20 mV/s. The current is normalized to the geometric area of the electrode.

A comparison of the electrochemical performance of ethanol oxidation on Pt-based electrodes in alkaline media is shown in Table 4. The peak current on our mesoporous Pt@CB is 18 mA/cm^2 and on Pt 8.4 mA/cm^2 which is higher than for all experiments in the work of Xu *et al.*[24] : Pt@CB 7 mA/cm^2, Pt 7.4 mA/cm^2 and Pt@CMS 12 mA/cm^2 (Pt supported on carbon microsphere). In our work the amount of Pt is 90 % higher than in the studies of Xu et *al.* [24, 38] explaining partially the differences in the mass activity. However, there is also a difference in the onset potentials, on our mesoporous Pt or Pt@CB, the onset potential is 120 mV lower than on the Pt based electrodes in the studies by Xu *et al.* A more than 100 mV reduction in the onset potential for an anodic reaction can be considered significant improvement for fuel cell applications. The anode reaction of the complete ethanol electro-oxidation reaction can be described as follows [3]:

$$CH_3CH_2OH + 3H_2O \rightarrow 2CO_2 + 12H^+ + 12e^- \tag{2}$$
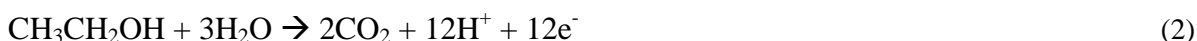
Furthermore, better catalytic activity towards ethanol oxidation has been observed at Pt(111) surface [26] which support our observation of mesoporous also having Pt(111) sites in the studies of cyclic voltammetry and CO adsorption (see above discussion). These result shows that the mesoporous Pt@CB electrocatalyst has higher activity than mesoporous Pt without carbon black supported for ethanol oxidation in alkaline media which could origin from differences in the morphologies. These results also show that this type of electrocatalyst is a promising candidate for ethanol sensors and direct ethanol fuel cells.

Table 4. Comparison of electrochemical performance of ethanol oxidation on Pt-based electrode in alkaline media with 1.0 M EtOH + 0.1 M NaOH.

Electrode	E_s/V	E_p/V	j_p/mA/cm^2	Pt loading/ (mg/cm^2)	Electrolyte with 1.0 M EtOH	Reference
Pt/C	0.43	0.76	7	0.1	0.1M KOH	[24]
Pt/CMS	0.43	0.76	12	0.1	0.1M KOH	[24]
Pt	0.24	0.72	7.4		0.1M KOH	[38]
Pt	0.25	0.75	8.4	0.5	0.1M NaOH	In this work
Pt@CB	0.31	0.82	18.2	1.0	0.1M NaOH	In this work

4. CONCLUSIONS

In this study, we have shown that mesoporous Pt and Pt@CB are good catalysts both in acidic and alkaline media, and especially for ethanol oxidation. Mesoporous Pt and Pt@CB were electrodeposited using both galvanostatic and potentiostatic methods from liquid crystal templates. Cryo-TEM, TEM, SAXS and SEM characterization showed that the structures are porous and after electrodeposition Pt stuctures have pores in the 3-5 nm size range. Cyclic voltammetry and CO adsorption/desorption were studied on the Pt and Pt@CB electrodes in both acid and alkaline media and both the samples had similar EASA. ORR experiments were done in acidic media (HClO$_4$), the results indicated that oxygen reduction proceeded readily on the galvanostatically prepared samples. The mass activities and onset potentials of mesoporous Pt (0.5 mg/m^2) is 2.4 A/g$_{Pt}$ and 0.91 V and

mesoporous Pt@CB (0.42 mg/m^2) is 2.6 A/g$_{Pt}$ and 0.98 V at 0.9 V vs. RHE at rotation rate of 2400 rpm. This results are better than for other Pt electrocatalysts reported in the literature. Moreover, ethanol oxidation in alkaline media was studied on mesoporous Pt and Pt@CB and the onset potentials of these samples were 0.24 V and 0.31 V which are lower than for other Pt based catalyst reported in the literature. More than 100 mV reduction in the onset potential for an anodic reaction can be considered significant improvement for fuel cell applications. The results showed that Pt@CB electrocatalyst have a high potential in direct ethanol fuel cells.

References

1. E. A. Franceschini, M. M. Bruno, F.A. Viva, F.J. Williams, M. Jobbagy and H. R. Corti, *Electrochim. Acta*, 71 (2012) 173
2. S.Shrestha, S. Ashegi, J. Timbro, C. M. Lang and W. E. Mustain, *ECS Transcations*, 41 (2011) 1183
3. A. Santasalo-Aarnio, S. Tuomi, K. Jalkanen, K. Kontturi and T. Kallio, *Electrochim. Acta*, 87 (2013) 730
4. N. Ramaswamy and S. Mukerjee, *Adv.Phys.Chem.*, (2012) 1
5. F.J. Perez-Alonso, D.N. McCarthy, A. Nierhoff, P. Hernandez-Fernandez, C. Strebel, I.E.L. Stephens, J.H. Nielsen and I. Chorkendorff, *Angew.Che.Int.Ed.*, 51 (2012) 4641
6. M. Arenz, K.J.J. Mayrhofer, V. Stamenkovic, B.B. Blizanac, T.T omoyuki, P.N. Ross, and N. M. Markovic, *J.Am.Chem.Soc.*, 127 (2005) 6819
7. H. Wang, M. Imura, Y .Nemoto, L. Wang, H.Y. Jeong, T. Yokoshima, O. Terasaki, and Y. Yamauchi, *Chem.Eur.J.,* 18 (2012) 13142
8. H. Wang, M. Imura, Y. Nemoto, L. Wang, H.Y .Jeong, T. Sato, Y. Sakamoto, S.T. Ominaka, K. Miyasaka, N. Miyamoto, Y. Nemoto, O. Terasaki, and Y. Yamauchi, *Chem.Mater.,* 24 (2012) 1591
9. G.S. Attard, C.G. Göltner, J.M. Corker, S. Henker, and R.H. Templer, *Angew.Chem.Int.Ed.Engl.,* 36 (1997) 1315
10. G.S. Attard, P.N. Bartlett, N.R.B. Coleman, J.M. Elliotl, J.R. Owen, and J.H. Wang, *Science,* 278 (1997) 838
11. G.S. Attard, P.N. Bartlett, N.R.B. Coleman, J.M. Elliot, and J.R. Owen, *Langmuir,* 14 (1998) 7340
12. J.M. Elliot, G.S. Attard, P.N. Bartlett, N.R.B. Coleman, D.A.S. Merckel, and J.R.Owen, *Chem.Mater.*, 11 (1999) 3602
13. P.R. Birkin, J.M. Elliot, and Y.E. Watson, *Chem.Commun.,* (2000) 1693
14. A. Bauer, D.P. Wilinson, E.L. Gyenge, D. Bizzotto and S.Ye, *J.Electrochem.Soc.,* 156 (2009) B1169
15. T.M. Bernhardt, U. Heiz, and U. Landman. *Nanocatalysis*., Springer Press, Berlin, (2007)
16. T. F. Esterle, A. E. Russel, and P. N. Bartlett, *Chem.Phys.Chem.,* 11 (2010) 2896
17. J. Kibsgaard, Y. Gorlin, Z. Chen, and T.F. Jaramillo, *J.Am.Chem.Soc.,* 134 (2012) 7758
18. S.-H. Liu, and J.-R. Wu, *Int.J.Electrochem.Sci.,* 7 (2012) 8326
19. D. Banham, F. Feng, K. Pei, S. Ye and V. Birss, *J.Mater.Chem.A*, 1 (2013) 2812

20. C. Liu, M. Chen, C. Du, J. Zhang, G. Yin, P. Shi, and Y. Sun, *Int.J.Electrochem.Sci.*, 7 (2012) 10592
21. M.-H. Chen, Y.-X. Jiang, S.-R. Chen, R. Huang, J.-L. Lin, S.-P. Chen and S.-G. Sun, *J.Phys.Chem. C*, 114 (2010) 19055
22. S. C. Lai and M.T.M. Koper, *Phys.Chem.Chem.Phys*., 11 (2009) 10446
23. A. Santasalo-Aarnioa, E. Sairainen, R.M. Arán-Ais, M.C. Figueiredo, J. Hua, J.M. Feliu, J. Lehtonen, R. Karinen, and T. Kallio, *J. Catal.*, 309 (2014) 38
24. C. Xu, L. Cheng, P. Shen, and Y. Liu, *Electrochem. Comm.*, 9 (2007) 997
25. C. Xu, Y. Su, L. Tan, Z. Liu, J. Zhang, S. Shen, and S.P. Jiang, *Electrochim. Acta*, 54 (2009) 6322
26. B. Pierozynski, *Int.J.Electrochem.Sci*., 7 (2012) 4261
27. Q.-S. Chen, J. Solla-Gullon, S.-G. Sun, and J. M. Feliu, *Electrochim. Acta*, 55 (2010) 7982
28. D. Chen, Q. Tao, L.W. Liao, S.X. Liu, Y.X. Chen, and S. Ye, *Electrocatal*., 2 (2011) 207
29. F.J. Vida-Iglesias, R.M. Aran-Ais, J. Solla-Gullon, E. Herrero and J. M.Feliu, *ACS Catal*., 2 (2012) 901
30. B. Krishnamurthy, and S. Deepalochani, *Int. J. Electrochem. Sci.*, 4 (2009) 386
31. A. Habrioux, D. Diabate, J. Rousseau, T.W. Napporn, K. Servat, L. Guetaz, A. Trokourey, and K.B. Kokoh, *Electrocatal*., 1 (2010) 51
32. M.C. Perez, A. Rincon, and C. Gutierrez, *J. Electroanal. Chem*., (2001) 39
33. C. Bock, and B. MacDougall, *J.Electrochem.Soc*. 150 (2003) E377
34. K.J.J. Mayrhofer, D. Strmcnik, B.B. Blizanac,V.R. Stamenkovic, M. Arenz, and N.M. Markovic, *Electrochm. Acta*, 53 (2008) 3181
35. A. Rodes, R. Gomez, J.M. Feliu, and M.J. Weaver. *Langmuir*, 16 (2000) 811
36. E. Higuchi, K. Adachi, S. Nohara, and H. Inoue, *Res.Chem.Intermed*., 35 (2009) 985
37. A. Kucernak, and J. Jiang, *Chem.Engin.J*., 93 (2003) 81
38. S.-W. Xie, S. Chen, Z.Q. Liu, and C.-W. Xu, *Int.J.Electrochem.Sci*., 6 (2011) 882